Crystal Structure of the L Protein of *Rhodobacter sphaeroides* Light-Independent Protochlorophyllide Reductase with MgADP Bound: A Homologue of the Nitrogenase Fe Protein[†,‡]

Ranjana Sarma,[§] Brett M. Barney,[||] Trinity L. Hamilton,[§] Alma Jones,[||] Lance C. Seefeldt,[||] and John W. Peters*[,§]

Department of Chemistry and Biochemistry and Astrobiology Biogeocatalysis Research Center, Montana State University, Bozeman, Montana 59717, and Department of Chemistry and Biochemistry, Utah State University, Logan, Utah 84322

Received June 4, 2008; Revised Manuscript Received October 13, 2008

ABSTRACT: The L protein (BchL) of the dark-operative protochlorophyllide reductase (DPOR) from *Rhodobacter sphaeroides* has been purified from an *Azotobacter vinelandii* expression system; its interaction with nucleotides has been examined, and the X-ray structure of the protein has been determined with bound MgADP to 1.6 Å resolution. DPOR catalyzes the reduction of protochlorophyllide to chlorophyllide, a reaction critical to the biosynthesis of bacteriochlorophylls. The DPOR holoenzyme is comprised of two component proteins, the dimeric BchL protein and the heterotetrameric BchN/BchB protein. The DPOR component proteins share significant overall similarities with the nitrogenase Fe protein (NifH) and the MoFe (NifDK) protein, the enzyme system responsible for reduction of dinitrogen to ammonia. Here, BchL was expressed in *A. vinelandii* and purified to homogeneity using an engineered polyhistidine tag. The purified, recombinant BchL was found to contain 3.6 mol of Fe/mol of BchL homodimer, consistent with the presence of a [4Fe-4S] cluster and analogous to the [4Fe-4S] cluster present in the Fe protein. The MgATP- and MgADP-induced conformational changes in BchL were examined by an Fe chelation assay and found to be distinctly different from the nucleotide-stimulated Fe release observed for the Fe protein. The recombinant BchL was crystallized with bound MgADP, and the structure was determined to 1.6 Å resolution. BchL is found to share overall structural similarity with the nitrogenase Fe protein, including the subunit bridging [4Fe-4S] cluster and nucleotide binding sites. Despite the high level of structural similarity, however, BchL is found to be incapable of substituting for the Fe protein in a nitrogenase substrate reduction assay. The newly determined structure of BchL and its comparison to its close homologue, the nitrogenase Fe protein, provide the basis for understanding how these highly related proteins can discriminate between their respective functions in microbial systems where each must function simultaneously.

Chlorophylls (Chl) and bacteriochlorophylls (Bch) are essential pigments involved in photosynthesis. The biosynthesis of both Chl and Bch in phototrophs starts from glutamate, which is converted to the photosynthetic pigment via 15 enzymatic steps. The rate-limiting step in this process involves reduction of a double bond of ring D of protochlorophyllide (Pchlide) to form chlorophyllide (Chlide) and can occur by either light-dependent or light-independent mechanisms (*1*−*3*). Light-dependent Pchlide reductase (LPOR, EC 1.3.1.33) has been extensively studied and is an NADPH- and light-dependent short chain dehydrogenase encoded by the *por* gene. This enzyme catalyzes a light-induced electron transfer and the formation of an ion radical of Pchlide (*2, 4, 5*). Light-independent (dark) Pchlide reductase (DPOR) exists as a two-component complex iron−sulfur enzyme encoded by the *bchL/chlL*, *bchB/chlB*, and *bchN/chlN* genes. In the light-independent reaction, the BchL/ChlL pair serves as a unique electron donor to a heterotetrameric complex of the BchB/ChlB and BchN/ChlN polypeptides, which contain the site for Pchlide reduction. The DPOR component proteins share considerable primary sequence identity with the Fe protein and MoFe protein of nitrogenase encoded by the *nifH*, *nifD*, and *nifK* genes (*2, 6*).

Nitrogenase catalyzes the reduction of molecular nitrogen to ammonia in a reaction requiring the hydrolysis of at least 16 equivalents of MgATP.[1] During nitrogenase catalysis, the Fe protein (NifH) and the MoFe protein associate and dissociate in a manner that couples the binding and hydrolysis of MgATP to sequential intercomponent electron transfer

[†] This work was supported by National Institutes of Health Grants GM069938 (J.W.P.) and GM59087 (L.C.S.). Portions of this research were carried out at the Stanford Synchrotron Radiation Laboratory (SSRL), a national user facility operated by Stanford University on behalf of the U.S. Department of Energy, Office of Basic Energy Sciences. The SSRL Structural Molecular Biology Program is supported by the Department of Energy, Office of Biological and Environmental Research, and by the National Institutes of Health, National Center for Research Resources, Biomedical Technology Program, and the National Institute of General Medical Sciences. The NASA Astrobiology Biogeocatalysis Research Center (NNA08CN85A) is supported by the NASA Astrobiology Institute.

[‡] The coordinates for this structure have been submitted to the RCSB Protein Data Bank (entry 3END).

* To whom correspondence should be addressed. Phone: (406) 994-7211. Fax: (406) 994-7212. E-mail: john.peters@chemistry.montana.edu.

[§] Montana State University.

[||] Utah State University.

10.1021/bi801058r CCC: $40.75
Published on Web 11/12/2008

events leading to substrate reduction at the FeMo cofactor substrate reduction sites located within the MoFe protein (NifDK) (*7, 8*). Structures of the Fe protein and the MoFe protein have been determined crystallographically (*8*−*13*) and studied using small-angle X-ray scattering (*14*). The Fe protein is a homodimer that binds MgATP and transfers electrons to MoFe concomitant with MgATP hydrolysis. The Fe protein contains one [4Fe-4S] cluster coordinated by four Cys residues, two from each subunit (*9*). The MoFe protein is an α_2/β_2 heterotetramer composed of NifD (α) and NifK (β) that contains two sets of metal clusters, the [8Fe-7S] P-cluster and the [1Mo-7Fe-9S-X-homocitrate] FeMo cofactor, the latter being the site for reduction of N_2 to NH_3 (*15*−*17*).

Amino acid sequence analysis has shown that the sequence of BchL is up to 30% identical and 50% overall similar with that of the Fe protein of nitrogenase (*18, 19*). The most notable regions of similarity are the ATP-binding motif and the Cys residues coordinating the [4Fe-4S] cluster that are invariant between the Fe protein and BchL (*18, 19*). EPR studies have indicated the presence of one [4Fe-4S] cluster per dimer of the BchL protein, similar to the cluster found in the Fe protein (*20*). The amino acid sequence of the N proteins (BchN/ChlN) and the B proteins (BchB/ChlB) share sequence similarity with NifD and NifK, respectively (*6, 21*). However, only four of the six Cys residues involved in forming the P-cluster in the MoFe protein are conserved in the N and B proteins, three in the N protein and one in the B protein (*22*). None of the residues involved in coordinating the FeMo cofactor in the MoFe protein are conserved in the BchNB, indicating that the active site of BchNB is highly divergent from the catalytic site of nitrogenase (*2, 6*).

There have been very limited biochemical studies on DPOR. *In vitro* assays have shown that BchL transfers electrons to the BchNB with the requirement of MgATP hydrolysis and a source of electrons, such as dithionite (*3*). From sequence comparison of Fe protein and BchL and mutagenesis of conserved residues in the phosphate binding loop (P loop) and switch regions of BchL from *Chlorobium tepidum*, key residues essential for catalysis have been identified (*23*). Although a homology model of BchL based the similarity of its sequence to that of the Fe protein has been proposed (*23*), a three-dimensional structure of the protein is essential for full characterization of the structural basis of the nucleotide-dependent electron transfer mechanism of the protein.

In this study, BchL from *Rhodobacter sphaeroides* has been expressed in the diazotroph *Azotobacter vinelandii*. BchL, with an engineered polyhistidine tag, was purified, and its interactions with nucleotides were characterized. A high-resolution crystal structure of BchL cocrystallized with MgADP has also been fully characterized. The key residues involved in nucleotide binding and cluster coordination have been identified on the basis of the three-dimensional structure. The overall topology and surface distribution of charges of BchL have been studied and compared to those of the Fe protein of nitrogenase, revealing important differences between BchL and the Fe protein at the docking surface. This study offers insights into the structural basis for the BchL function and mechanisms by which BchL and the highly related nitrogenase Fe protein discriminate between their respective macromolecular partners.

EXPERIMENTAL PROCEDURES

Materials Used. All reagents were obtained from Sigma-Aldrich (St. Louis, MO) and were used as provided unless specified otherwise. Nitrogenase Fe protein was expressed and purified from strain DJ884 as previously described (*24*). Cells of *A. vinelandii* were grown on a derivation of Burk's medium (final concentrations of 60 mM sucrose, 800 μM $MgSO_4 \cdot 7H_2O$, 600 μM $CaCl_2 \cdot 2H_2O$, 18 μM $FeSO_4 \cdot 7H_2O$, 1 μM $Na_2MoO_4 \cdot 2H_2O$, 1.5 mM KH_2PO_4, and 4.5 mM K_2HPO_4) that was supplemented with fixed nitrogen as either ammonium acetate (2.6 mM) or urea (concentrations of up to 10 mM). Where appropriate, streptomycin (0.5 mg/L) was included in solid medium (1.3% bacto-agar).

Construction of an A. vinelandii Expression Strain. A plasmid was designed that allowed the *bchL* gene to be inserted behind the Mo-dependent nitrogenase structural gene promoter within the *A. vinelandii* chromosomal DNA in place of the *nifH* gene. In this way, BchL expression could be controlled by the removal of a fixed nitrogen source in a background protected from oxygen inactivation and with FeS cluster biosynthetic proteins. A strain of *A. vinelandii* (DJ764) was kindly provided by D. Dean (Virginia Tech, Blacksburg, VA), which has a deletion of the *nifH* gene. In addition, a plasmid was constructed from parent plasmid pDB613 (from D. Dean), which contains a 460 bp segment of DNA upstream of the *nifH* start codon and that had been modified to contain an *Nde*I site with the start codon ATG as the second half of the *Nde*I sequence (CATATG), and also a 1570 bp segment of *nifK* downstream of the *Nde*I site. These two segments were selected to serve as flanking regions for incorporating genes into the *A. vinelandii* genomic copy of the *nifH* operon. The plasmid is based on a pUC parental plasmid containing an ampicillin cassette for selection in *Escherichia coli*. This plasmid is incapable of replication in *A. vinelandii* and thus serves as an ideal suicide transfer vector. Several additional modifications were made, using standard molecular biology techniques, to fill in and delete the *Bam*HI and *Bgl*II sites lying at each end of the flanking regions. Once removed, a *Bam*HI site and a *Bgl*II site were both incorporated behind the *Nde*I site. The *Bgl*II site, which was downstream from the *Bam*HI site, was then utilized to incorporate a gene cassette containing resistance markers for spectinomycin and streptomycin by digesting plasmid pHP45Omega with *Bam*HI and inserting it into the *Bgl*II site of the construct. This incorporation removed the *Bgl*II site and maintained the single *Bam*HI following the *Nde*I site to move genes of interest into this expression vector. Finally, two additional restriction sites were incorporated into the expression vector by first removing an extra *Xba*I site from the region outside the flanking regions and then introducing an *Nsi*I site immediately downstream of *Nde*I and an *Xba*I site 13 bases downstream of the *Nsi*I site. The completed vector (pBB044) has two sites (*Nde*I or *Nsi*I) for use as the start codon insertion site and two sites (*Xba*I

[1] Abbreviations: MgADP, magnesium adenosine 5′-diphosphate; MgATP, magnesium adenosine 5′-triphosphate; EPR, electron paramagnetic resonance; PCR, polymerase chain reaction; SDS, sodium dodecyl sulfate; NCS, noncrystallographic symmetry; TLS, translation/libration/screw; SSM, secondary structure matching; APBS, Adaptive Poisson−Boltzmann Solver.

or *Bam*HI) that are all unique and can be utilized to shuttle genes into this completed construct. Two specific primers [BBP139 (5′CCGCCCTGCAGCTCCCGTCGATGG) and BBP365 (5′GCAATAGTTGGCGAAGTAATCGCAACATC-CGC)] binding upstream of the *Nde*I site and complementary to the region downstream of the *Bam*HI were designed to sequence genes through this segment of DNA to confirm correct incorporation of the genes once inserted and have been used for successful DNA sequencing of completed plasmid constructs.

Construction of the BchL Expression Vector. The *R. sphaeroides* (strain 2.4.1) was kindly provided by J. Williams (Arizona State University, Tempe, AZ) and was grown on LB medium. Cells were collected, and the DNA was isolated by rupturing the cells with Triton X-100 and lysozyme in a Tris-HCl buffer at pH 8.0. The cells were boiled for 5 min and then sedimented at 12000 *g* to pellet any debris. Genomic DNA was precipitated by adding an equal volume of 2-propanol to the supernatant. The pellet was washed once with 2-propanol and then again with ethanol before being dried in air. The DNA was resuspended in buffer and further processed by digestion with selected restriction enzymes (NE Biolabs, Ipswich, MA) and purification following the Qiaex II (Qiagen, Valencia, CA) DNA desalting protocol. The *bchL* gene was amplified by PCR from the purified genomic DNA using primers BBP101 (5′GACGGTACCGAGTTGGAA-GACCGTCTCGAGGGGATTG) and BBP118 (5′GTAC-G A A T T C G T C G T T C A T G G G T T C T T C C T - TGAACACCGG), where the underlined region represents a *Kpn*I site. The PCR product was then purified and digested with *Kpn*I (in primer BBP101) and *Bam*HI (downstream of primer BBP118) and inserted into pUC19. The plasmid was then further modified to incorporate an *Nde*I site into the start codon, and a seven-polyhistidine tag into the N-terminus, followed by an *Nco*I site. This results in the entire gene, with the sequence MHHHHHHG in place of the initial methionine. The gene was then transferred to pBB044, and the entire *bchL* gene region was sequenced within this plasmid to confirm that there were no mistakes. The final constructed plasmid pPCRBchL4 was used for the transformation of *A. vinelandii*.

DNA was introduced into *A. vinelandii* strains made competent using a procedure similar to that described by Page and von Tigerstrom (*25*).

Purification of BchL. Cells of Av-BchL4 were grown in a 100 L fermentor at the Center for Integrated Biosystems at Utah State University using Burk's medium (above) supplemented with 10 mM urea. The cells were grown while the urea concentration was monitored, in solution. Gene expression directed by the *nifH* promoter is repressed in the presence of a fixed nitrogen source. Thus, for the initial growth of cells, urea at 10 mM was included in the growth medium. Upon adequate growth (an optical density of at least 0.6 at 600 nm) during the initial phase, the cells were harvested and resuspended in a medium devoid of fixed nitrogen. The absence of fixed nitrogen in the medium results in derepression of the *nifH* promoter and expression of the genes for nitrogen fixation. Since BchL was substituted for NifH, it is expressed under these conditions. Cells were grown for an additional 5 h for maximal expression of BchL.

All purification steps were performed in the absence of oxygen under argon utilizing degassed buffers supplemented with 2 mM sodium dithionite, similar to the techniques used to purify the MoFe protein of nitrogenase from *A. vinelandii* (*26*). Briefly, cells were resuspended in a buffer containing glycerol (37%, v/v) in Tris-HCl buffer at pH 7.9. These were allowed to mix for 10 min, and then the cells were sedimented at 8000*g* for 15 min. The supernatant was removed; 2 mg of DNase was added to the cell pellet, and the cells were rapidly resuspended in a Tris-HCl buffer (pH 7.9) without glycerol while steps to minimize oxygen introduction were taken, resulting in an osmotic shock of the cells that ruptured the cell membrane. The cell debris was sedimented by centrifugation at 50000*g* for 30 min, and the supernatant was applied to a zinc-loaded chelating Sepharose fast flow (GE Healthcare, Uppsala, Sweden) chromatography column with a bed volume of 300 mL and equilibrated with Tris-HCl buffer (pH 7.9) containing 500 mM NaCl. The column was then washed with the same Tris buffer containing 30 mM imidazole, and the protein eluted with the same Tris buffer containing 500 mM imidazole. The fractions containing BchL were combined and diluted in 50 mM Tris buffer (pH 7.9) to lower the overall salt concentration to <100 mM. The solution was then loaded on a Q-Sepharose (GE Healthcare) column with a bed volume of approximately 200 mL, where it bound to the top of the column as a dark band. The column was washed with 1 column volume of Tris buffer (pH 7.9) to remove the remaining imidazole, and then the protein was eluted with a continuous gradient of NaCl (from 100 to 500 mM) while fractions were collected. Fractions containing BchL were combined and concentrated and then frozen in liquid nitrogen for later use. The purified BchL protein was judged to be greater than 85% pure on the basis of analysis by SDS gels stained with Coomassie blue. The molecular mass was determined by mass spectroscopy to be 33376.7 Da, which is in good agreement with the predicted mass of 33311.8 Da from the sequence. Protein concentrations were determined by the Biuret method with bovine serum albumin (BSA) as the standard. All manipulation of proteins was done in septum-sealed serum vials under an argon atmosphere, and gas and liquid transfers were conducted with gastight syringes. BchL was used at final concentrations near 85 mg/mL.

Determination of Iron Content with α,α′-Dipyridyl. Four reagent solutions were prepared in distilled water: (i) 5 mM $Fe(NH_4)_2(SO_4)_2 \cdot 2H_2O$, (ii) 5% HCl, (iii) 10% hydroxylamine, and (iv) 20 mM α,α′-dipyridyl. Iron standards were prepared by using solution (i) with appropriate dilutions. For the Fe determination of BchL protein, 5, 10, or 20 μL of an 85 mg/mL protein stock was added to different test tubes. Distilled water was added to each to bring the final volume to 400 μL in each tube; 100 μL of solution (ii) was added to each tube. The tubes were incubated at 80 °C for 10 min and then allowed to cool to room temperature. The reactions were initiated by adding 1.275 mL of distilled water, 100 μL of solution (iii), and 125 μL of solution (iv) to each sample. The tubes were allowed to incubate at room temperature for 45 min while the color developed. The absorbance was measured at 520 nm, and the Fe^{2+} content was determined from the Fe standard curve.

MgATP-Dependent Release of Fe^{2+} from Wild-Type Fe Protein and BchL. The time-dependent reaction of the Fe protein or BchL with the iron chelator α,α′-dipyridyl was

carried out as described by Walker and Mortenson (*27, 28*). Fe protein or BchL (1.4 mg) was added to a 1 cm path length cuvette fitted with a rubber septum and containing an argon-saturated solution of 35 mM Tris buffer (pH 7.5), 6.25 mM α,α′-dipyridyl, 1.3 mM sodium dithionite, and 150 mM NaCl in a total volume of 1 mL. MgATP was added from a freshly prepared solution of 300 mM Tris-HCl (pH 7.5), 1.3 mM sodium dithionite, 200 mM ATP, and 300 mM $MgCl_2$ in a total volume of 5 mL. For each addition of MgATP, 40 μL of this MgATP solution was added to each cuvette. The first injection of the MgATP solution resulted in final concentrations of 3.9 mM ATP and 5 mM $MgCl_2$. The absorbance at 520 nm was monitored as a function of time for a total of 300 s prior to and after the injection of MgATP relative to a reference cuvette with no added protein. For MgADP addition, a freshly prepared solution of 300 mM Tris-HCl (pH 7.5), 1.3 mM sodium dithionite, 200 mM ADP, and 300 mM $MgCl_2$ in a total volume of 5 mL was used. For addition of MgADP, 40 μL of the MgADP solution was added to the cuvette during each injection. The first injection of MgADP resulted in final concentrations of 3.9 mM ADP and 5 mM $MgCl_2$. Absorbance at 520 nm versus time for 200 s prior to and after the injection of MgADP was monitored.

Nitrogenase Association and Competition Experiments. In an effort to assess the ability of BchL to interact with the nitrogenase MoFe protein, nitrogenase assays for reduction of protons to dihydrogen were performed as described. The rates for proton reduction were determined in 9 mL sealed vials with a liquid volume of 1 mL using established protocols for 10 min at 30 °C. The assay liquid contained a MgATP regeneration system (5 mM ATP, 6 mM $MgCl_2$, 30 mM phosphocreatine, and 0.2 mg/mL creatine phosphokinase), in a MOPS buffer at pH 7.0 (100 mM) with 1.2 mg/mL BSA, and 9 mM dithionite. Solutions were degassed with oxygen-free argon. MoFe protein was added first (10 μL of a 10 mg/mL stock) followed by Fe protein (10 μL of a 20 mg/mL stock) to initiate the reaction. The reaction was quenched by the addition of 300 μL of 400 mM EDTA. Dihydrogen in the headspace of quenched samples was assessed by gas chromatography with a molecular sieve 5A column with argon as a carrier gas and a thermal conductivity detector.

Protein Crystallization and Data Collection. Purified BchL was diluted to a final concentration of 30 mg/mL in 50 mM Tris buffer (pH 7.8) with 350 mM NaCl and 2 mM dithionite prior to crystallization. The conditions for crystallization were initially identified using sparse matrix screens (*29*). Crystals were grown under anaerobic conditions in a nitrogen atmosphere glovebox (UniLAB, MBRAUN, NH) using a microcapillary batch diffusion method (*9*) with 20−25% PEG 3350 as the precipitating agent, with 200 mM magnesium formate (pH 7.7). A final concentration of 10 mM MgADP was added to the protein prior to crystallization. BchL cocrystallized with MgADP, with crystals appearing in 3−4 weeks as brown-colored long rods with dimensions of ∼600 μm × 50 μm × 50 μm. The crystals were flash-cooled in liquid nitrogen on rayon loops, and data were collected on beamline 9-2 at the Stanford Synchrotron Radiation Laboratory under a continuous flow of liquid nitrogen at 100 K. A single-wavelength data set was collected ($\lambda = 0.95$) up to a resolution 1.6 Å. The data were integrated using *DENZO* and scaled using *SCALPACK* of the HKL2000 software package (*30*), and the unit cell parameters and data statistics are summarized in Table 1. Calculation of the Matthews coefficient (*31, 32*) and consideration of the reasonable solvent content of the crystals suggested that each asymmetric unit likely contains one BchL dimer.

Table 1: Diffraction Statistics

cell dimensions	$a = 56.73$ Å $b = 86.62$ Å $c = 117.17$ Å $\alpha = \beta = \gamma = 90.00°$
space group	$P2_12_12_1$
wavelength (λ_1)	0.95376
resolution (Å)	50−1.6
completeness (%)	96.6 (96.4)[a]
no. of observed reflections	273732
no. of unique reflections	133747 (13313)[a]
average redundancy	2.0 (2.0)[a]
I/σ	40 (4.6)[a]
R_{sym} (%)[b]	3.7 (24.2)[a]
Refinement statistics	
resolution (Å)	50−1.6
R_{cryst}[c] (%)	17.3
R_{free}[c] (%)	19.8
real space CC[d] (%)	96.3
mean B value (overall) (Å^2)	14.64
coordinate error (Å)	0.049
root-mean-square deviation from ideality	
bonds (Å)	0.008
angles (deg)	1.183
Ramchandran plot[e]	
most favored (%)	98.68
additional allowed (%)	1.32

[a] Numbers in parentheses refer to the highest-resolution shell. [b] $R_{sym} = 100\sum_h\sum_i|I_i(h) - \langle I(h)\rangle|/\sum_h I(h)$, where $I_i(h)$ is the ith measurement of reflection h and $\langle I(h)\rangle$ is the average value of the reflection intensity. [c] $R_{cryst} = \sum||F_o| - |F_c||/\sum|F_o|$, where F_o and F_c are the observed and calculated structure factor amplitudes used in refinement, respectively. R_{free} is calculated as R_{cryst}, but using the "test" set of structure factor amplitudes that were withheld from refinement. [d] The correlation coefficient (CC) is agreement between the model and $2mF_o - DF_c$ electron density map. [e] Calculated using Molprobity (*54*).

Structure Determination and Refinement. On the basis of the high level of sequence similarity (*18, 19*) and presumed structural homology between the Fe protein and BchL, it was fair to assume structural similarity between the Fe protein and BchL. A molecular replacement approach using the Fe solution as a search was employed for structure determination. Molecular replacement was accomplished using AutoMR of the CCP4 suite of programs (*33*) with one dimer of the MgADP-bound Fe protein (PDB entry 1FP6) (*12*) as a search model. The best solution was subjected to rigid body refinement in REFMAC5 (*34*), resulting in R_{cryst} and R_{free} of approximately 50%. The model was improved using *ARP/wARP* (*35*) run in the *Classic* mode using data from 50 to 1.6 Å and a total of 10 building cycles. *ARP/wARP* resulted in successfully building approximately 58% of the model. At this stage, the [4Fe-4S] cluster was added to the model; solvent flattening and histogram matching using RESOLVE (*36*) were used to improve the map quality allowing building of the reset of the model using COOT (*37*), and subsequent refinement (REFMAC5) resulted in a well-determined structure.

Both subunits in the structure have clear and unambiguous density for residues 30−297, for one [4Fe-4S] cluster, and one MgADP molecule per subunit. The N-terminus (1−29) on both the subunits was not resolved in electron density maps even after several rounds of refinement. The final model

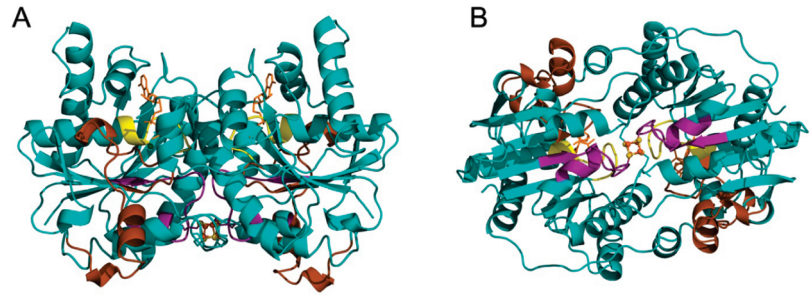

FIGURE 1: Overall structure. (A) Ribbon diagram of the BchL dimer, showing the mixed α-helix−β-sheet topology. The cluster is shown in ball and stick representation, with the Fe atoms colored rust and the sulfur atoms orange. The ADP is colored orange as a stick representation, and the Mg^{2+} is depicted as a forest green sphere. The P loop is colored yellow, switch I brown, and switch II purple. The 2-fold symmetric axis runs parallel to the plane of the page and vertically between the subunits. (B) Alternate view of the protein, looking down the 2-fold axis, showing the [4Fe-4S] cluster and the four coordinating Cys residues, two from each subunit.

was refined to an R_{cryst} of 17.3% and an R_{free} of 19.8% (Table 1). The refinement runs made use of NCS restraints, *B*-factor restraints, and 11 screw (TLS) tensors (per polypeptide chain). The final model obeys good stereochemistry with 100% of the residues in the allowed regions of the Ramachandran plot (*38*). Figures 1−5 were generated using PyMOL (*39*), and the electrostatics were calculated using Adaptive Poisson−Boltzmann Solver (APBS) (*40*). The Fe protein was superimposed on BchL in Figure 3 for direct comparisons of surface charge in specific orientations.

Annotated amino acid sequences included in the Fe protein and BchL alignment were downloaded from the National Center for Biotechnology Institute (NCBI), and the alignments were generated with CLUSTALW using the residue numbers for Fe protein. Secondary structure assignment for the aligned sequences was derived using PROCHECK (*38*) on the BchL structure file. The accession numbers for the amino acid sequences used for generating Figure 2B are ZP_00417477 (*A. vinelandii*) and YP_353362 (*R. sphaeroides*).

RESULTS AND DISCUSSION

Properties of BchL. An *A. vinelandii* strain (Av-BchL4) was constructed that allows BchL from *R. sphaeroides* to be expressed under the control of the *nifH* promoter from within the *A. vinelandii* chromosome. Expression of BchL in this system was initiated by the removal of all fixed nitrogen from actively growing Av-BchL4 cells. The expressed BchL, with a polyhistidine tag, was purified to near homogeneity using a metal affinity chromatography protocol. The total Fe content of the purified BchL was determined by an α,α′-dipyridyl assay with hydroxylamine. For comparison, a sample of purified Fe protein was analyzed at the same time. On the basis of the concentration and molecular mass of the two proteins, the amount of iron found was 3.5 mol of iron/mol of Fe protein and 3.6 mol of iron/mol of BchL homodimer. These findings are consistent with previous studies (*20*) indicating the presence of one [4Fe-4S] cluster per BchL dimer.

Interaction of BchL with the Nitrogenase MoFe Protein. It has been shown that nitrogenase components from different sources were compatible in a nitrogenase *in vitro* assay (*41*). These studies revealed that the Fe protein from *Rhodospirillum rubrum*, which is significantly similar in sequence to that of *R. sphaeroides*, was able to support nitrogen fixation with the MoFe protein from *A. vinelandii*. Because BchL is also homologous, albeit to a lesser extent, to the Fe protein, the ability of BchL to serve as an electron donor to the MoFe protein of *A. vinelandii* was investigated using a standard nitrogenase proton reduction assay under an argon atmosphere with a MgATP regeneration system.

In this assay, Fe protein from *A. vinelandii* was used as a positive control, and the molar ratio of Fe protein to MoFe protein was held at 8:1. Dihydrogen formation was followed by analysis using a gas chromatograph with a thermal conductivity detector as an indication of proton reduction activity. This analysis was selected, as it is the default reduction performed by nitrogenase in the absence of any other substrate. When BchL was substituted for the Fe protein in these experiments, at the same molar ratio, no sign of dihydrogen formation was found. In a different experiment, it was determined that BchL did not interfere with the normal functioning of the Fe protein and MoFe protein in proton reduction. In this experiment, varying amounts of BchL were added to an Fe protein−MoFe protein assay and the effects on proton reduction rates were compared to controls containing no BchL. Even at a BchL:MoFe protein ratio of 20:1, no inhibition of proton reduction was observed. These results indicate that the BchL is not able to associate with the MoFe protein, even transiently. It has been shown that the purple non-sulfur bacteria *Rhodobacter capsulatus* is capable of fixing nitrogen during photosynthetic growth (*42*). The inability of BchL to support transfer of electrons to the MoFe protein or even associate in a competitive manner may indicate that these organisms separate bacteriochlorophyll biosynthesis from nitrogen fixation and effectively direct reducing equivalents to these processes independently.

Cluster Accessibility to Fe Chelation. On the basis of earlier studies, BchL is proposed to contain a [4Fe-4S] cluster and to have a nucleotide binding site on each subunit, just like the Fe protein (*20, 23*). An important property of the Fe protein is that MgATP binding to the protein induces protein conformational changes in the protein that result in the exposure of the Fe atoms of the [4Fe-4S] cluster to metal chelators. This can easily be followed by the time-dependent increase in absorbance for the formation of an α,α′-dipyridyl−Fe^{2+} complex stimulated by the addition of MgATP to the Fe protein. The accessibility of the FeS cluster of BchL was examined in such an Fe chelation assay, and the impact of the addition of MgATP on the chelation rate was determined. BchL showed no significant Fe chelation rate in the absence of MgATP and a very slow chelation

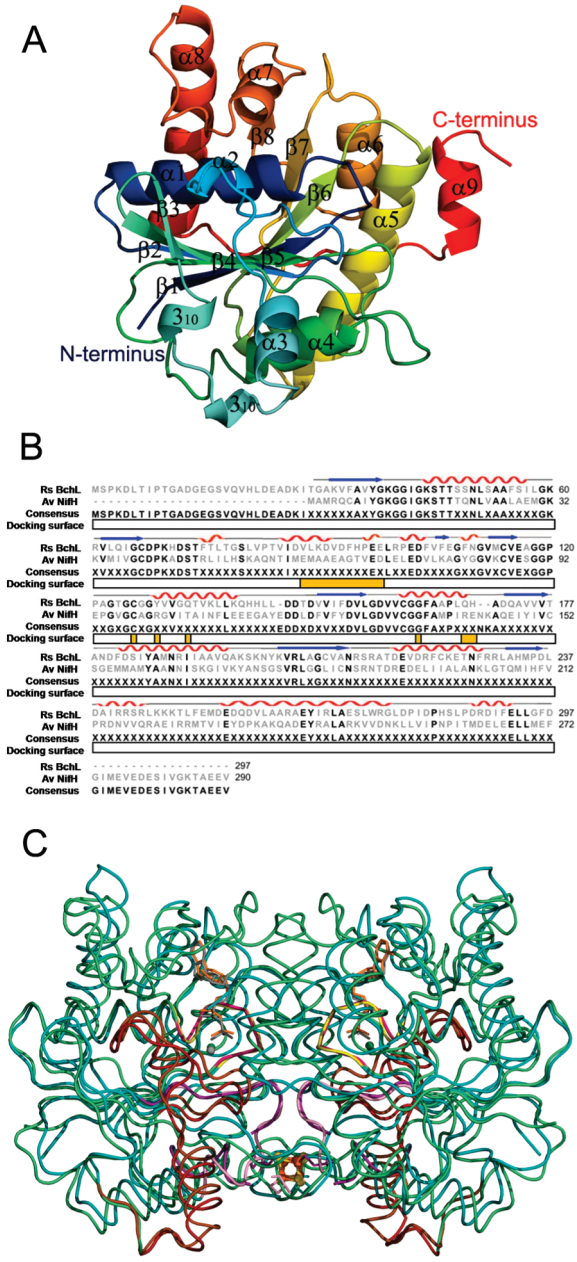

FIGURE 2: (A) Color ramp of secondary structure elements in rainbow colors with blue representing residues closer to the N-terminus and red representing the C-terminal end. The residue ranges for the secondary structure elements were calculated using STRIDE (*55*). (B) Amino acid sequence alignment of BchL from *R. sphaeroides* and Fe protein of *A. vinelandii*. The secondary structure presented is that of BchL. The residues highlighted using the yellow bar represent the residues of the Fe protein implicated in interacting with the MoFe protein and the analogous residues in BchL. (C) Loop representation of the BchL dimer cocrystallized with MgADP superimposed on the Fe protein dimer cocrystallized with MgADP (*12*). The overall BchL dimer is colored cyan, the P loop yellow, switch I brown, and switch II purple. The cluster is shown in ball-and-stick representation with Fe atoms colored rust and sulfur atoms orange. The ADP molecule is shown as orange sticks, and Mg^{2+} is shown as green spheres. The overall Fe dimer is colored cyan, the P loop yellow-orange, switch I pink, and switch II violet. The cluster is shown in ball-and-stick representation and colored uniformly cyan. The ADP molecule is colored light blue, and Mg^{2+} is shown as cyan spheres.

rate in the presence of MgATP. This contrasts with the significant Fe chelation observed for the Fe protein upon addition of MgATP. The addition of MgADP instead of

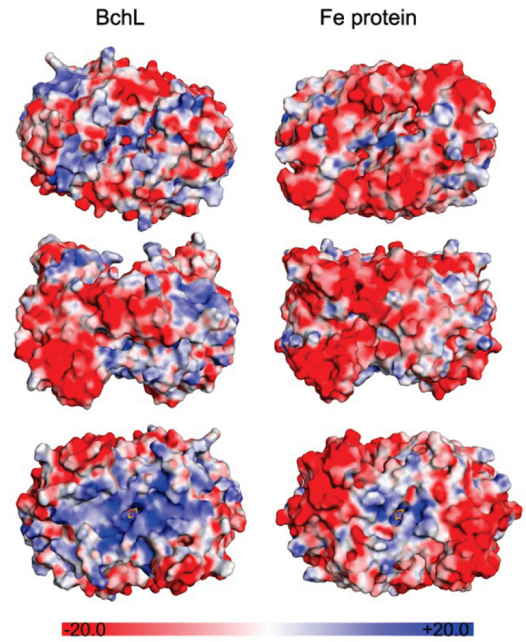

Table of residues on the docking surface

Analogous residues on the docking surface of BchL	Residues of Fe protein involved in interaction with MoFe protein
Cys126	Cys97
Tyr129	Arg100
Gln133	Thr104
Gly161	Gly133
Gln168	Arg140
His169	Glu141

FIGURE 3: Relative distribution of charges of BchL (left panels) and Fe protein (right panels) surfaces calculated using APBS (*40*). The three different views represent perspectives separated by 90° about the horizontal axis, including views of the nucleotide binding face (top), side view (middle), and the [4Fe-4S] cluster face (bottom). The scale shows the charge distribution from −20 to 20 *kT/e*, where red represents negatively charged residues and blue represents positively charged residues. The table compares the specific residues of the Fe protein involved in formation of the nitrogenase complex with analogous residues in BchL.

MgATP in a parallel assay did not elicit any significant Fe chelation for either the BchL or Fe proteins over the time frame that was tested.

Overall Structure. The structure of *R. sphaeroides* BchL cocrystallized with MgADP has been determined and refined to 1.6 Å. BchL is a dimer of identical subunits in its quaternary structure with each subunit having an α/β domain (Figure 1), very similar to the Fe protein of nitrogenase (*9, 10*). Each subunit has eight β-sheets at the core of the protein, flanked by nine α-helices (Figure 2A). The twisted β-sheet core of each subunit has an 8−7−6−1−5−2−4−3 strand order, with the core five β-strands (6−1−5−2−4) arranged as parallel sheets and three β-strands (8, 7, and 3) arranged in an orientation antiparallel to the five core β-strands. Comparison of the secondary structure of BchL with that of the Fe protein shows that the strand order of the β-sheet core is exactly the same between the two proteins (*10*) with the same antiparallel strand, β_3 at the edge of the β-sheet core. The [4Fe-4S] cluster is positioned on the 2-fold symmetric axis of the protein and is coordinated by residues from each of the subunits (Figure 1B). This cluster is symmetrically coordinated by two Cys residues from each subunit, Cys126

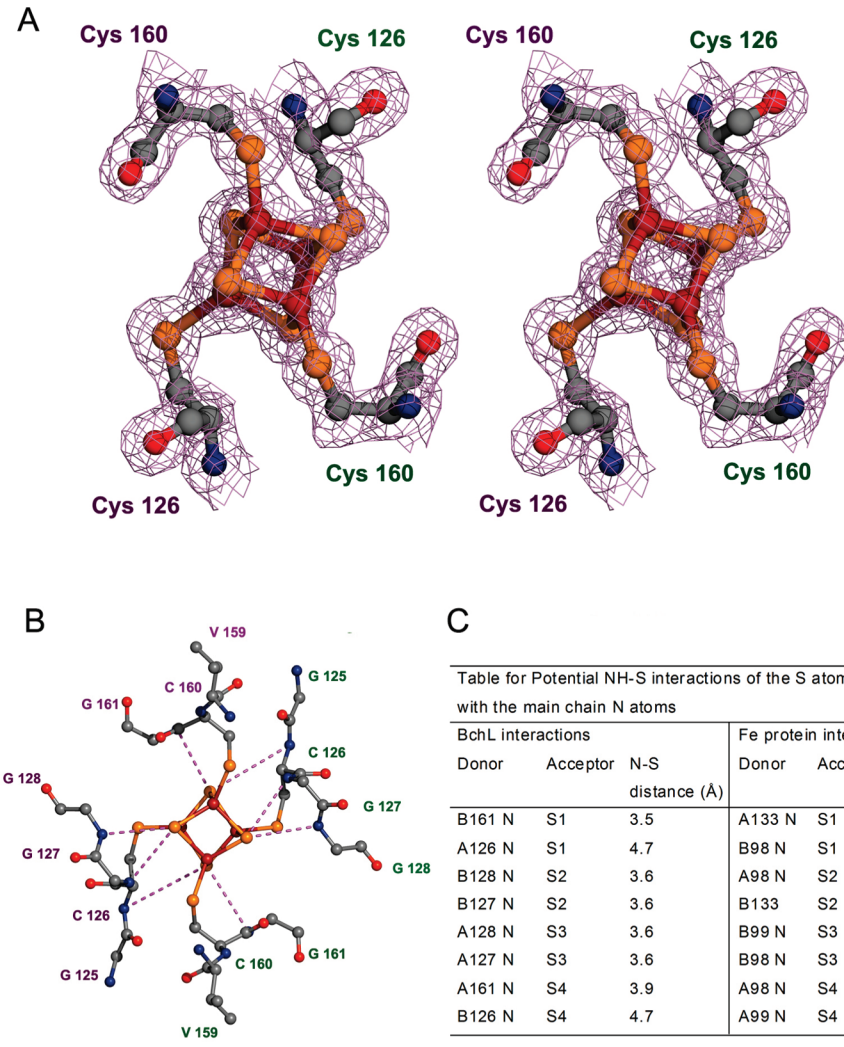

C

Table for Potential NH-S interactions of the S atoms of the cluster with the main chain N atoms

BchL interactions			Fe protein interactions		
Donor	Acceptor	N-S distance (Å)	Donor	Acceptor	N-S distance (Å)
B161 N	S1	3.5	A133 N	S1	3.8
A126 N	S1	4.7	B98 N	S1	4.5
B128 N	S2	3.6	A98 N	S2	4.4
B127 N	S2	3.6	B133	S2	3.8
A128 N	S3	3.6	B99 N	S3	3.8
A127 N	S3	3.6	B98 N	S3	3.7
A161 N	S4	3.9	A98 N	S4	4.0
B126 N	S4	4.7	A99 N	S4	3.9

FIGURE 4: (A) Stereoview of a $2F_o - F_c$ map calculated for the [4Fe-4S] cluster and the coordinating Cys residues. The map is contoured at 1.0σ. (B) Ball-and-stick representation of the [4Fe-4S] cluster environment of BchL cocrystallized with MgADP viewed down the 2-fold symmetric axis. The potential stabilizing NH−S bonds are represented by dashed lines colored magenta. In both panels, residues from chain A are labeled in green and those from chain B in purple. (C) Table listing the potential NH−S bonds between the [4Fe-4S] cluster and the protein main chain of the Fe protein and BchL.

and Cys160, which is analogous to the coordination of the [4Fe-4S] cluster of the Fe protein. The Cys residues involved in cluster coordination are conserved between BchL and the Fe protein as seen in amino acid sequence alignments (Figure 2B). The cluster face of the Fe protein interacts directly with the MoFe protein during formation of the nitrogenase complex (*8, 11*), bringing the [4Fe-4S] cluster into the proximity of the P-cluster facilitating transfer of electrons to the FeMo cofactor. Presumably, BchL and BchNB function in an analogous manner in bacteriochlorophyll biosynthesis with the putative docking surface of BchL that interacts with the BchNB also occurring on the cluster face of the protein.

In spite of the similarities between the overall protein topology between BchL and the Fe protein cocrystallized with MgADP (*12*), there are several subtle differences in their quaternary structures that can be estimated by secondary structure matching (SSM). Estimates of root-mean-square deviations (rmsd) in the C^α positions between the two proteins were calculated using the protein structure comparison service SSM at European Bioinformatics Institute (http://www.ebi.ac.uk/msd-srv/ssm) (*43*). SSM of the individual subunits of BchL with the individual subunits of the Fe protein results in rmsd estimates of 1.6 Å in the C^α positions with a *q*-square of 0.6 and a total match of ~255 residues. Superimposition of the dimer of BchL onto the dimer of the Fe protein gives an overall rmsd of 1.9 Å, perhaps reflecting slight differences in the relative juxtaposition of the subunits of the two proteins with respect to one another. High estimates of rmsd in C^α positions and the regions of highest variability in the secondary structures of BchL and the Fe protein align very well with the regions of high *B*-factor observed for each of the two proteins.

Upon close inspection of the C^α trace of the BchL dimer superimposed on the C^α trace of the Fe protein dimer, it is observed that the regions of sequence conservation are also conserved in the quaternary structure (Figure 2C). The switch regions, P loop, and [4Fe-4S] cluster interface are among the most conserved regions between the two protein structures, and this is observed when the two sequences are aligned (Figure 2B). The dimer interface between the two subunits in both BchL and the Fe protein seems to overlay each other with significant similarities in main chain residue positions. The orientation of the MgADP molecule is quite similar in both proteins as observed when BchL is superimposed on the Fe protein cocrystallized with MgADP (*12*)

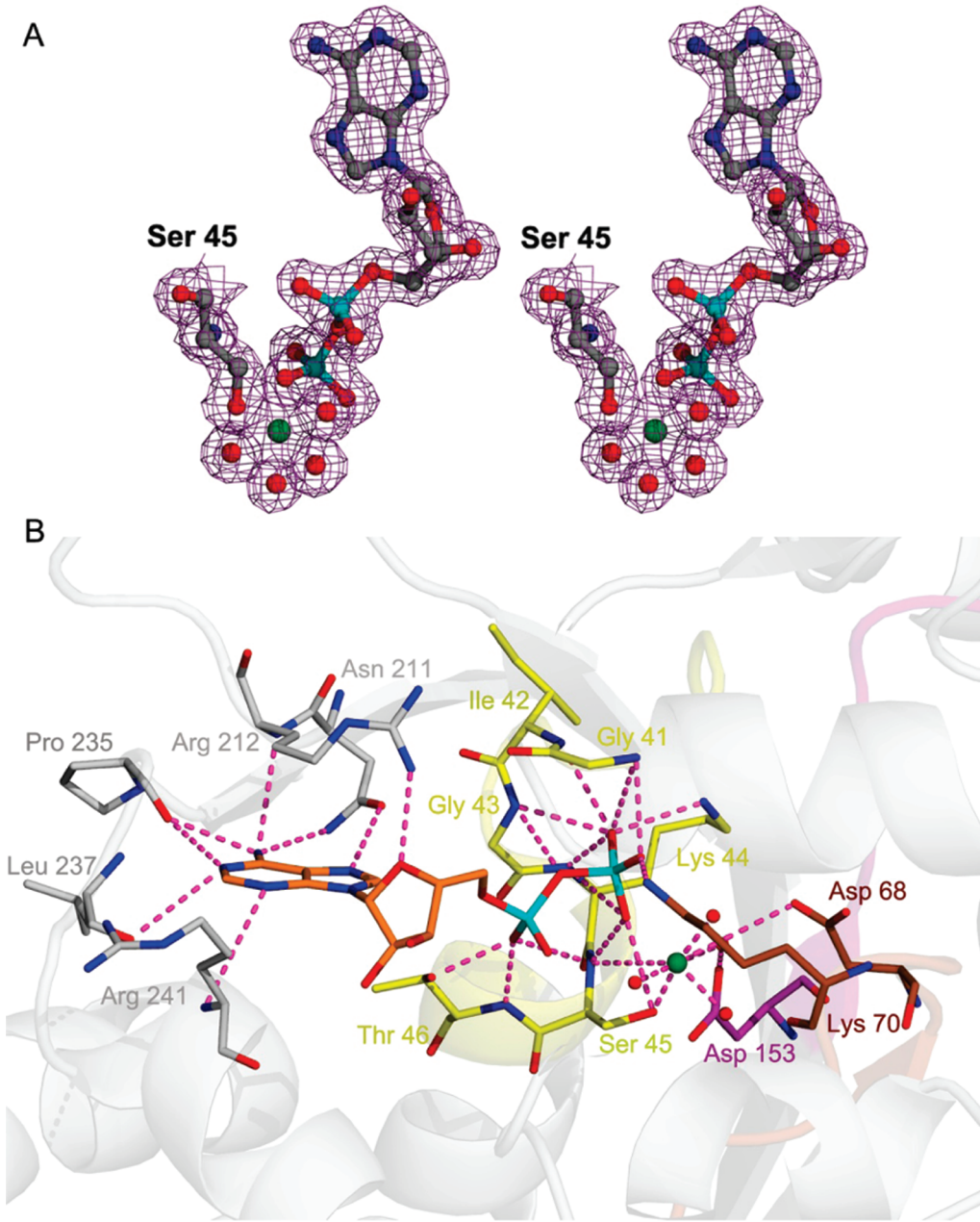

FIGURE 5: (A) Stereoview of the $2F_o - F_c$ map calculated for the MgADP molecule. The Mg^{2+} is colored green, and the coordinating water molecules are shown as isolated oxygen molecules colored red. The phosphates are colored cyan and the nitrogen atoms blue. Ser45 from the P loop is shown. The map is contoured at 1.0σ. (B) Stick representation of main chain and side chain interactions at the MgADP binding site. The residues from the P loop are colored yellow, those from the switch I region brown, and those from the switch II region purple. The ADP molecule is colored orange with the nitrogen atoms colored blue, oxygen atoms red, and phosphorus atoms cyan. The Mg^{2+} is colored green, and the coordinating water molecules are shown as isolated oxygen molecules colored red. In all the residues, the nitrogen atoms are colored blue and the oxygen atoms red. The protein backbone is shown as a ribbon in the background. All hydrogen bonds are shown as dashed lines colored magenta.

(Figure 2C). However, the interactions of the nucleotide with the main chain and side chain residues of the protein differ in the Fe protein compared to BchL, which is further elaborated later.

The subtle differences in the overall shape and surface of the Fe protein and BchL are evident from the surface representations in Figure 3. In these surface-rendered representations of BchL and the Fe protein, salient features of the structures can be observed. The differences in overall shape between the two proteins and most notably the differences in the distribution of surface charges on BchL and Fe protein surface are clearly seen in Figure 3. Despite these differences, the calculated isoelectric point (pI) of BchL, 5.21, is very similar to the pI of the Fe protein, 4.68, determined using the same method (*44*).

[4Fe-4S] Cluster Environment. As in the case of the Fe protein, a single [4Fe-4S] cluster is positioned on the 2-fold symmetric axis of BchL and is coordinated by the thiol ligands of Cys126 and Cys160 from each subunit. At the resolution of this structure, clear density for each iron atom and each sulfur atom can be discerned (Figure 4A). The cluster environment consists primarily of residues in the regions of positions 124−128, 158−162, and switch II (153−164). Most of the interactions between the cluster and the protein residues are in the form of NH−S bonds. The sulfur atoms of the cluster are poised to form potential NH−S

bonds with the amide nitrogen of adjacent residues, Gly127, Gly128, and Gly161 (Figure 4B,C). The NH−S interactions of the cluster in the Fe protein cocrystallized with MgADP (*12*) are observed to be similar to the NH−S interaction of the BchL cluster. Residues in the Fe protein, viz., Ala98, Gly99, and Gly133, analogous to Gly residues of BchL, are poised to form potential hydrogen bonds with the sulfur atoms of the cluster.

As observed in the Fe protein (*12*), the [4Fe-4S] cluster in BchL is located near the surface of the putative docking face. The cluster is protected by the residues of the loop connecting β4 and α4 and the loop connecting β5 and the following 3_{10}-helix. Also, the region surrounding the [4Fe-4S] cluster is predominantly positively charged. In the Fe protein, the cluster is similarly solvent exposed with residues from the loop connecting β4 and α3 and the loop connecting β5 and the following 3_{10}-helix surrounding the cluster and enclosing it in a positively charged pocket. On the basis of these similarities, it would be predicted that the midpoint reduction potential for the $[4Fe\text{-}4S]^{2+/+}$ couple of BchL would be similar to that reported for the Fe protein (−300 mV vs NHE) (*45*). Phe135 in the switch II region of Fe protein which has been implicated in modulating the midpoint potential of the [4Fe-4S] cluster (*46*) is conserved in the switch II region of BchL (Phe163).

Nucleotide Binding Site. The structure of BchL was obtained by cocrystallizing the protein with MgADP. During refinement, one MgADP molecule was placed into a nucleotide binding pocket in each subunit. The two nucleotide binding pockets in the Fe protein and in other related nucleotide binding proteins are characterized by three core elements (*10, 47, 48*): (a) the β-sheet core flanked by α-helices, (b) the phosphate-binding P loop, and (c) the two switch regions that interact with the γ-phosphate of the nucleotide and the Mg^{2+}. The P loop region is characterized by the classic GXXXXGKS/T sequence or Walker A motif (*49*), found as residues 38−46 in BchL. The refinement quality, the high resolution, and the quality of the final maps show that the MgADP is present at high occupancy in each of the subunits (Figure 5A). The MgADP molecules on each of the subunits are located near the dimer interface, parallel to the 2-fold symmetric axis (Figure 1A). The β-phosphates are oriented toward the [4Fe-4S] cluster, in an orientation similar to what is observed in the MgADP-bound structure of the Fe protein (*12*). The entry of MgADP into the nucleotide binding sites is from the protein face opposite to the face housing the [4Fe-4S] cluster. Channels leading into the nucleotide binding pocket end in regions of significant negative charge. The bulk of these negative charges is provided by aspartate residues from the switch I and switch II regions (Asp68, Asp72, and Asp153), which are involved in the coordination of the Mg^{2+} ions, either directly or indirectly through water molecules.

The important interactions of the MgADP molecule with the protein main chain and side chain atoms in BchL (Figure 5B) have been compared to the analogous interactions observed in the Fe protein (*12*) and are listed in Table 2. Some of the differences observed include the interactions of the phosphates of the ADP with the residues of the P loop and switch I and II regions in the BchL structure that are slightly more extensive than that observed in the Fe protein structure. The residues making up the P loop and the nucleotide switch regions I and II have been assigned on the basis of sequence conservation between BchL and analogous regions in the Fe protein, and these assignments are supported by BchL mutagenesis studies (*23*).

Table 2: Main Chain and Side Chain Interactions at the MgADP Site (Distances in Angstroms)

BchL interactions		Fe protein interactions	
base		base	
Asn211($O_{\delta1}$)−ADP(N7)	2.9	Asn185($O_{\delta1}$)−ADP(N7)	3.1
Asn211($N_{\delta1}$)−ADP(N6)	2.9	Asn185($N_{\delta1}$)−ADP(N6)	3.2
Arg212(N)−ADP(N6)	3.6	Gln236($N_{\epsilon1}$)−ADP(N6)	3.2
		Tyr240(OH)−ADP(N6)	3.7
Pro235(O)−ADP(N6)	2.9	Pro212(O)−ADP(N6)	2.9
Pro235(O)−ADP(N1)	3.6	Asp214(N)−ADP(N1)	3.2
Leu237(N)−ADP(N1)	3.0	Asp214(O)−ADP(N1)	3.4
Arg241(N)−ADP(N3)	4.0	Gln218($O_{\epsilon1}$)−ADP(N1)	3.1
ribose			
Arg212(NH1)−ADP(O4*)	3.07		
phosphate		phosphate	
Gly41(N)−ADP(O1 B)	3.5	Gly12(N)−ADP(O1 B)	3.5
Ile42(N)−ADP(O1 B)	3.2	Ile13(N)−ADP(O1 B)	3.5
Gly43(N)−ADP(O1 B)	3.0	Gly14(N)−ADP(O1 B)	3.3
Lys44(N)−ADP(O1 B)	2.8	Lys15(N)−ADP(O1 B)	3.0
Lys44(N_ζ)−ADP(O1 B)	2.9	Lys15(N_ζ)−ADP(O1 B)	3.0
Gly41(N)−ADP(O2 B)	2.9	Gly12(N)−ADP(O2 B)	3.1
Lys70(N_ζ)−ADP(O2 B)	2.9		
Lys44(N)−ADP(O3 B)	3.6	Lys15(N)−ADP(O3 B)	3.6
Ser45(N)−ADP(O3 B)	2.9	Ser16(N)−ADP(O3 B)	3.0
Ser45(O_γ)−ADP(O3 B)	2.9	Ser16(O_γ)−ADP(O3 B)	3.1
Lys44(N)−ADP(O1 A)	4.2		
Ser45(N)−ADP(O2 A)	3.3	Ser16(N)−ADP(O2 A)	3.0
Thr46(O_γ)−ADP(O2 A)	2.7	Thr17(O_γ)−ADP(O2 A)	3.2
Thr46(N)−ADP(O2 A)	2.8	Thr17(N)−ADP(O2 A)	2.8
Gly43(N)−ADP(O3 A)	3.2	Gly14(N)−ADP(O3 A)	3.2
Mg^{2+}		Mg^{2+}	
Ser45(O_γ)−Mg^{2+}	2.1	Ser16(O_γ)−Mg^{2+}	2.3
Ser45(N)−Mg^{2+}	3.9	Ser16(N)−Mg^{2+}	4.1
Asp68($O_{\delta2}$)−Mg^{2+}	3.8	Asp39($O_{\delta2}$)−Mg^{2+}	3.9

The interactions between the protein main chain and the phosphates of the ADP molecule along with the protein interactions with the adenine ring are important for maintaining the right orientation of the ADP molecule. The Mg^{2+} is coordinated by three water molecules and Oγ of Ser45 at the equatorial positions (Figure 5B). Residues 66−74 make up switch I which is proposed to communicate nucleotide binding and its hydrolysis to the putative docking surface. This region interacts with the nucleotide through N_ζ of Lys70 which forms a hydrogen bond with O_2 of the β-phosphate and through O_γ of Asp68 which interacts with Mg^{2+}. The switch II region of BchL (residues 153−164) is predicted to be responsible for communicating nucleotide binding and hydrolysis to the [4Fe-4S] cluster. In analogy to the role of Asp125 in the Fe protein, Asp153 detects different nucleotide-bound states by hydrogen bonding to a water molecule coordinated to the Mg^{2+}. The nucleotide binding site is linked to the [4Fe-4S] cluster via Asp153 and cluster ligand Cys160.

The entrance to the nucleotide binding pocket in BchL is well-protected by the residues from the loop connecting β7 and α6 and the loop connecting β8 and α7. These loops are oriented toward the opening to the nucleotide binding pocket, together covering the entrance. The opening to the nucleotide binding pocket in the Fe protein is slightly larger than in BchL. The loop connecting β8 and α7 in the Fe protein is positioned similar to the loop connecting β8 and α7 in BchL; however, the loop connecting β7 and α6 in the Fe protein is oriented away from the entrance to the nucleotide binding pocket (Figure 2A). Another noticeable difference between

the nucleotide binding regions of the two proteins is the extent of positive charge surrounding the entrance to the channels leading into the nucleotide binding pocket. BchL is predominantly positively charged around the entrance to the nucleotide binding pocket, and this predominance of positive charge is not observed in the Fe protein (Figure 3).

Docking Surface. Previously characterized structures of the Fe protein−MoFe protein complex (*8, 11*) and the L127ΔFe protein−MoFe protein complex (*13*) have revealed that Cys97, Arg100, Thr104, Gly133, Arg140, and Glu141 of the Fe protein interact directly with residues of the MoFe protein during formation of the nitrogenase complex. Interestingly, except for Cys97 and Gly133, these residues are not conserved between the Fe protein and BchL, and amino acid sequence alignments and structural comparisons indicate that residues Cys126, Tyr129, Glu133, Gly161, Glu168, and His169 of BchL reside in analogous positions. The aforementioned residues have largely differing chemical character and are consistent with the analysis of surface charge of the Fe protein and BchL indicating a significantly different distribution of charge present at their respective docking faces (Figure 3). As mentioned previously, the docking face of BchL is significantly more uniformly positively charged that the Fe protein. This positively charged small patch of residues is surrounded by neutral residues in BchL with negative charge present only at the periphery. In contrast, the bulk of the docking face of the Fe protein is composed of negatively charged residues with the exception of a small region of positive charge in the region of the [4Fe-4S] cluster.

The region of switch I including residues 59−69 of the Fe protein has also been implicated as being important in MoFe protein interactions (*50*). In this region of switch I in BchL (residues 88−100), the residues are of a very different nature compared to those of the Fe protein. In place of three alanine residues in Fe protein, there are aspartate residues in the BchL protein, and small side chains of Gly65, Thr66, and Val67 observed in the Fe protein are present as bulky residues in the analogous positions in BchL, viz., Phe94, His95, and Pro96. These observations are consistent with the biochemical results indicating that BchL cannot supplant the activity of the Fe protein or does not even compete with the Fe protein in *in vitro* nitrogenase assays. The significant differences observed at the docking surface would result in the incompatibility of the two systems (nitrogen fixation and dark bacteriochlorophyll biosynthesis). Interestingly, although our biochemical results clearly indicate that Fe protein and BchL are not functionally interchangeable, it has been reported that the BchL-related ChlL can be substituted with the Fe protein *in vivo* in the green alga *Chlamydomonas reinhardtii* (*54*). The level at which the Fe protein can support ChlL activity is not reported in this study, however, but in line with our conclusions, there would be no selective pressure to adapt discreet discrimination between these proteins since green algae do not fix nitrogen.

In addition to the DPOR system, there are several less characterized enzymatic systems homologous to the nitrogenase system, namely, the COR system (BchXYZ proteins) (*51, 52*), which, like DPOR, also catalyzes the reduction of a double bond in chlorophyll biosynthesis, and the Nfl proteins (*53*), whose exact function remains unclear. Further characterization of the COR system and Nfl proteins will most likely reveal the structural differences that result in specific interaction of their component proteins and will further elucidate key differences between these homologous enzyme systems that allow each to specifically and exclusively interact with their partner proteins. The notable differences between the docking surface of BchL and the Fe protein might serve to discriminate the otherwise common architecture found in these homologous proteins and thus enable their exclusive interaction with partner proteins. Because these enzyme systems may be coexpressed in many organisms, COR and DPOR in phototrophic diazotrophs and Nfl proteins in methanogenic diazotrophs, and because the reactions these systems catalyze are energy-dependent, the ability of organisms to efficiently and exclusively shuttle energy and electrons to the necessary enzymatic systems would be highly dependent on the ability of these related systems to operate independently without unproductive cross talk. The comparison of the Fe protein and BchL structures described herein indicates that key differences in the regions of the proteins that support formation of the complex are the basis for discriminating electron flow to their respective substrates.

SUMMARY AND CONCLUSIONS

In this study, BchL from *R. sphaeroides* expressed in *A. vinelandii* has been purified to near homogeneity. The structural and biochemical characterization of BchL and the subsequent comparisons to the Fe protein indicate that there are a number of features that are common to both proteins as anticipated but also reveal interesting key difference in the biochemical properties and structural features. The results indicate similar iron content and a similar structural environment of the [4Fe-4S] cluster for both BchL and the Fe protein; however, they exhibit distinct differences in the susceptibility of the cluster to the MgATP-dependent iron chelation with the BchL exhibiting significantly lower susceptibility in comparison to the Fe protein. While BchL and the Fe protein share many common structural features, BchL was unable to substitute for the role for the Fe protein in nitrogenase assays. The overall structure of BchL is very similar to that of the Fe protein, although there are some differences in the overall shape of the two proteins and significant differences in surface charge especially at the sites for protein−protein interactions with their respective partners (BchNB and MoFe protein). These studies provide a strong foundation for future mutagenesis experiments for probing the role of specific amino acid residues in discriminating their respective functions.

ACKNOWLEDGMENT

The authors thank Dr. Joann Williams from Arizona State University for *R. sphaeroides* and Dr. Dennis Dean from Virginia Tech for *A. vinelandii* strains.

REFERENCES

1. Armstrong, G. A. (1998) Greening in the dark: Light-independent chlorophyll biosynthesis from anoxygenic photosynthetic bacteria to gymnosperms. *J. Photochem. Photobiol., B 43*, 87–100.
2. Fujita, Y. (1996) Protochlorophyllide reduction: A key step in the greening of plants. *Plant Cell Physiol. 37*, 411–421.
3. Fujita, Y., and Bauer, C. E. (2000) Reconstitution of light-independent protochlorophyllide reductase from purified bchl and BchN-BchB subunits. In vitro confirmation of nitrogenase-like

features of a bacteriochlorophyll biosynthesis enzyme. *J. Biol. Chem. 275*, 23583–23588.
4. Willows, R. D. (2003) Biosynthesis of chlorophylls from protoporphyrin IX. *Nat. Prod. Rep. 20*, 327–341.
5. Lebedev, N., and Tinko, M. (1998) Protochlorophyllide photoreduction. *Photosynth. Res. 58*, 5–23.
6. Fujita, Y., Matsumoto, H., Takahashi, Y., and Matsubara, H. (1993) Identification of a *nif*DK-like gene (ORF467) involved in the biosynthesis of chlorophyll in the cyanobacterium *Plectonema boryanum*. *Plant Cell Physiol. 34*, 305–314.
7. Rees, D. C., and Howard, J. B. (2000) Nitrogenase: Standing at the crossroads. *Curr. Opin. Chem. Biol. 4*, 559–566.
8. Schindelin, H., Kisker, C., Schlessman, J. L., Howard, J. B., and Rees, D. C. (1997) Structure of ADP•AlF_4^--stabilized nitrogenase complex and its implications for signal transduction. *Nature 387*, 370–376.
9. Georgiadis, M. M., Komiya, H., Chakrabarti, P., Woo, D., Kornuc, J. J., and Rees, D. C. (1992) Crystallographic structure of the nitrogenase iron protein from *Azotobacter vinelandii*. *Science 257*, 1653–1659.
10. Schlessman, J. L., Woo, D., Joshua-Tor, L., Howard, J. B., and Rees, D. C. (1998) Conformational variability in structures of the nitrogenase iron proteins from *Azotobacter vinelandii* and *Clostridium pasteurianum*. *J. Mol. Biol. 280*, 669–685.
11. Tezcan, F. A., Kaiser, J. T., Mustafi, D., Walton, M. Y., Howard, J. B., and Rees, D. C. (2005) Nitrogenase complexes: Multiple docking sites for a nucleotide switch protein. *Science 309*, 1377–1380.
12. Jang, S. B., Seefeldt, L. C., and Peters, J. W. (2000) Insights into nucleotide signal transduction in nitrogenase: Structure of an iron protein with MgADP bound. *Biochemistry 39*, 14745–14752.
13. Chiu, H., Peters, J. W., Lanzilotta, W. N., Ryle, M. J., Seefeldt, L. C., Howard, J. B., and Rees, D. C. (2001) MgATP-bound and nucleotide-free structures of a nitrogenase protein complex between the Leu 127ΔFe-protein and the MoFe-protein. *Biochemistry 40*, 641–650.
14. Sarma, R., Mulder, D. W., Brecht, E., Szilagyi, R. K., Seefeldt, L. C., Tsuruta, H., and Peters, J. W. (2007) Probing the MgATP-bound conformation of the nitrogenase Fe protein by solution small-angle X-ray scattering. *Biochemistry 46*, 14058–14066.
15. Peters, J. W., and Szilagyi, R. K. (2006) Exploring new frontiers of nitrogenase structure and mechanism. *Curr. Opin. Chem. Biol. 10*, 101–108.
16. Howard, J. B., and Rees, D. C. (2006) How many metals does it take to fix N_2? A mechanistic overview of biological nitrogen fixation. *Proc. Natl. Acad. Sci. U.S.A. 103*, 17088–17093.
17. Barney, B. M., Lee, H. I., Dos Santos, P. C., Hoffman, B. M., Dean, D. R., and Seefeldt, L. C. (2006) Breaking the N_2 triple bond: Insights into the nitrogenase mechanism. *Dalton Trans.,* 2277–2284.
18. Suzuki, J. Y., and Bauer, C. E. (1992) Light-independent chlorophyll biosynthesis: Involvement of the chloroplast gene *chlL* (*frxC*). *Plant Cell 4*, 929–940.
19. Burke, D. H., Hearst, J. E., and Sidow, A. (1993) Early evolution of photosynthesis: Clues from nitrogenase and chlorophyll iron proteins. *Proc. Natl. Acad. Sci. U.S.A. 90*, 7134–7138.
20. Nomata, J., Kitashima, M., Inoue, K., and Fujita, Y. (2006) Nitrogenase Fe protein-like Fe-S cluster is conserved in L-protein (BchL) of dark-operative protochlorophyllide reductase from *Rhodobacter capsulatus*. *FEBS Lett. 580*, 6151–6154.
21. Fujita, Y., Takagi, H., and Hase, T. (1996) Identification of the *chlB* gene and the gene product essential for the light-independent chlorophyll biosynthesis in the cyanobacterium *Plectonema boryanum*. *Plant Cell Physiol. 37*, 313–323.
22. Nomata, J., Ogawa, T., Kitashima, M., Inoue, K., and Fujita, Y. (2008) NB-protein (BchN-BchB) of dark-operative protochlorophyllide reductase is the catalytic component containing oxygen-tolerant Fe-S clusters. *FEBS Lett. 582*, 1346–1350.
23. Brocker, M. J., Virus, S., Ganskow, S., Heathcote, P., Heinz, D. W., Schubert, W. D., Jahn, D., and Moser, J. (2008) ATP-driven reduction by dark-operative protochlorophyllide oxidoreductase from *Chlorobium tepidum* mechanistically resembles nitrogenase catalysis. *J. Biol. Chem. 283*, 10559–10567.
24. Seefeldt, L. C., Morgan, T. V., Dean, D. R., and Mortenson, L. E. (1992) Mapping the site(s) of MgATP and MgADP interaction with the nitrogenase of *Azotobacter vinelandii*. Lysine 15 of the iron protein plays a major role in MgATP interaction. *J. Biol. Chem. 267*, 6680–6688.
25. Page, W. J., and von Tigerstrom, M. (1979) Optimal conditions for transformation of *Azotobacter vinelandii*. *J. Bacteriol. 139*, 1058–1061.
26. Christiansen, J., Goodwin, P. J., Lanzilotta, W. N., Seefeldt, L. C., and Dean, D. R. (1998) Catalytic and biophysical properties of a nitrogenase Apo-MoFe protein produced by a *nifB*-deletion mutant of *Azotobacter vinelandii*. *Biochemistry 37*, 12611–12623.
27. Walker, G. A., and Mortenson, L. E. (1974) Effect of magnesium adenosine 5′-triphosphate on the accessibility of the iron of clostridial azoferredoxin, a component of nitrogenase. *Biochemistry 13*, 2382–2388.
28. Walker, M. N., and Mortenson, L. E. (1974) Evidence for the existence of a fully reduced state of molybdoferredoxin during the functioning of nitrogenase, and the order of electron transfer from reduced ferredoxin. *J. Biol. Chem. 249*, 6356–6358.
29. Cudney, R., Patel, S., Weisgraber, K., Newhous, Y., and McPhearson, A. (1994) Screening and optimization strategies for macromolecular crystal growth. *Acta Crystallogr. D50*, 414–423.
30. Otwinowski, Z., and Minor, W. (1997) Processing of X-ray diffraction data collected in oscillation mode. In *Macromolecular Crystallography* (Carter, C. W., Jr., and Sweet, R. M., Eds.) pp 307−326, Academic Press, Inc., New York.
31. Matthews, B. W. (1968) Solvent content of protein crystals. *J. Mol. Biol. 33*, 491–497.
32. Kantardjieff, K. A., and Rupp, B. (2003) 'Matthews' coefficient probabilities: Improved estimates for unit cell contents of proteins, DNA, and protein-nucleic acid complex crystals. *Protein Sci. 12*, 1865–1871.
33. Collaborative Computational Project No. 4 (1994) The CCP4 suite: Programs for protein crystallography. *Acta Crystallogr. D50*, 760–763.
34. Murshudov, G. N., Vagin, A. A., and Dodson, E. J. (1997) Refinement of macromolecular structures by the maximum-likelihood method. *Acta Crystallogr. D53*, 240–255.
35. Perrakis, A., Morris, R., and Lamzin, V. S. (1999) Automated protein model building combined with iterative structure refinement. *Nat. Struct. Biol. 6*, 458–463.
36. Terwilliger, T. C. (2003) SOLVE and RESOLVE: Automated structure solution and density modification. *Methods Enzymol. 374*, 22–37.
37. Emsley, P., and Cowtan, K. (2004) Coot: Model-building tools for molecular graphics. *Acta Crystallogr. D60*, 2126–2132.
38. Laskowski, R. A., Macarthur, M. W., Moss, D. S., and Thornton, J. M. (1993) Procheck: A Program to Check the Stereochemical Quality of Protein Structures. *J. Appl. Crystallogr. 26*, 283–291.
39. DeLano, W. L. (2002) PyMol, DeLano Scientific, San Carlos, CA.
40. Baker, N. A., Sept, D., Joseph, S., Holst, M. J., and McCammon, J. A. (2001) Electrostatics of nanosystems: Application to microtubules and the ribosome. *Proc. Natl. Acad. Sci. U.S.A. 98*, 10037–10041.
41. Emerich, D. W., and Burris, R. H. (1978) Complementary functioning of the component proteins of nitrogenase from several bacteria. *J. Bacteriol. 134*, 936–943.
42. Kern, M., Kamp, P. B., Paschen, A., Masepohl, B., and Klipp, W. (1998) Evidence for a regulatory link of nitrogen fixation and photosynthesis in *Rhodobacter capsulatus*via HvrA. *J. Bacteriol. 180*, 1965–1969.
43. Krissinel, E., and Henrick, K. (2004) Secondary-structure matching (SSM), a new tool for fast protein structure alignment in three dimensions. *Acta Crystallogr. D60*, 2256–2268.
44. Gasteiger, E., Hoogland, C., Gattiker, A., Duvaud, S., Wilkins, M. R., Appel, R. D., andBairoch, A. (2005) *Protein Identification and Analysis Tools on the ExPASy Server*, Humana Press Totowa, NJ.
45. Watt, G. D., Wang, Z. C., and Knotts, R. R. (1986) Redox Reactions of and Nucleotide Binding to the Iron Protein of *Azotobacter vinelandii*. *Biochemistry 25*, 8156–8162.
46. Ryle, M. J., Lanzilotta, W. N., and Seefeldt, L. C. (1996) Elucidating the mechanism of nucleotide-dependent changes in the redox potential of the [4Fe-4S] cluster in nitrogenase iron protein: The role of phenylalanine 135. *Biochemistry 35*, 9424–9434.
47. Milner-White, E. J., Coggins, J. R., and Anton, I. A. (1991) Evidence for an ancestral core structure in nucleotide-binding proteins with the type A motif. *J. Mol. Biol. 221*, 751–754.
48. Sprang, S. R. (1997) G protein mechanisms: Insights from structural analysis. *Annu. Rev. Biochem. 66*, 639–678.
49. Walker, J. E., Saraste, M., Runswick, M. J., and Gay, N. J. (1982) Distantly related sequences in the α- and β-subunits of

ATP synthase, myosin, kinases and other ATP-requiring enzymes and a common nucleotide binding fold. *EMBO J. 1*, 945–951.
50. Peters, J. W., Fisher, K., and Dean, D. R. (1994) Identification of a nitrogenase protein-protein interaction site defined by residues 59 through 67 within the *Azotobacter vinelandii* Fe protein. *J. Biol. Chem. 269*, 28076–28083.
51. Burke, D. H., Alberti, M., and Hearst, J. E. (1993) The *Rhodobacter capsulatus* chlorin reductase-encoding locus *bchA*, consists of three genes, *bchX*, *bchY*, and *bchZ*. *J. Bacteriol. 175*, 2407–2413.
52. Nomata, J., Mizoguchi, T., Tamiaki, H., and Fujita, Y. (2006) A second nitrogenase-like enzyme for bacteriochlorophyll biosynthesis: Reconstitution of chlorophyllide a reductase with purified X-protein (BchX) and YZ-protein (BchY-BchZ) from *Rhodobacter capsulatus*. *J. Biol. Chem. 281*, 15021–15028.
53. Raymond, J., Siefert, J. L., Staples, C. R., and Blankenship, R. E. (2004) The natural history of nitrogen fixation. *Mol. Biol. Evol. 21*, 541–554.
54. Davis, I. W., Leaver-Fay, A., Chen, V. B., Block, J. N., Kapral, G. J., Wang, X., Murray, L. W., Arendall, W. B., III, Snoeyink, J., Richardson, J. S., and Richardson, D. C. (2007) MolProbity: All-atom contacts and structure validation for proteins and nucleic acids. *Nucleic Acids Res. 35*, W375–W383.
55. Frishman, D., and Argos, P. (1995) Knowledge-based protein secondary structure assignment. *Proteins 23*, 566–579.

BI801058R